

BROADBAND OBSERVATIONS OF THE GAMMA-RAY EMITTING NARROW LINE SEYFERT 1 GALAXY SBS 0846+513

VAIDEHI S. PALIYA^{1,2}, BHOOMIKA RAJPUT¹, C. S. STALIN¹, AND S. B. PANDEY³

¹Indian Institute of Astrophysics, Block II, Koramangala, Bangalore-560034, India

²Department of Physics, University of Calicut, Malappuram-673635, India and

³Aryabhata Research Institute of Observational Sciences, Manora peak, Nainital-263129, India

ApJ accepted

ABSTRACT

We present the results of our broadband study of the γ -ray emitting narrow line Seyfert 1 (NLSy1) galaxy SBS 0846+513 ($z = 0.585$). This includes multi-band flux variations, γ -ray spectral analysis, broad band spectral energy distribution (SED) modeling, and intranight optical variability (INOV) observations carried over 6 nights between 2012 November and 2013 March using the 2 m Himalayan Chandra Telescope and the 1.3 m telescope at Devasthal. Multiple episodes of flaring activity are seen in the γ -ray light curve of the source which are also reflected in the observations at lower frequencies. A statistically significant curvature is noticed in the seven years averaged γ -ray spectrum, thus indicating its similarity with powerful flat spectrum radio quasars (FSRQs). Modeling the SEDs with a one zone leptonic emission model hints the optical-UV spectrum to be dominated by synchrotron radiation, whereas, inverse Compton scattering of broad line region photons reproduces the γ -ray part of the SEDs. The source was found to be variable on all the six nights of optical observations with a variation of ~ 0.3 magnitude within a single night, coinciding with a high γ -ray activity state. The observed large amplitude INOV clearly indicates the presence of a closely aligned beamed relativistic jet in SBS 0846+513. Our broadband study supports the recent claims in literature that γ -ray emitting NLSy1 galaxies are similar to blazars and constitute the low black hole mass counterparts to FSRQs.

Subject headings: galaxies: active — galaxies: individual (SBS 0846+513) — galaxies: Seyfert — gamma-rays: general

1. INTRODUCTION

The high energy extragalactic γ -ray sky, as seen by the *Fermi* Gamma-ray Space Telescope, is dominated by the blazar class of active galactic nuclei (AGN, e.g., Ackermann et al. 2015). Along with blazars, significant γ -ray emission is also observed from about half-a-dozen radio-loud narrow line Seyfert 1 (RL-NLSy1) galaxies (e.g., Abdo et al. 2009; Foschini 2011; D’Ammando et al. 2012; Yao et al. 2015). NLSy1 galaxies are a sub-class of AGN with peculiar properties that distinguishes them from the conventional broad line Seyfert 1 galaxies. For example, their optical spectra consist of narrow Balmer lines (FWHM (H_β) < 2000 km s⁻¹), weak [O III] ([O III]/ $H_\beta < 3$), and strong optical Fe II lines (Osterbrock & Pogge 1985; Goodrich 1989). They exhibit rapid X-ray flux variations (Pounds et al. 1995) and steep soft X-ray spectra (Boller et al. 1996). It is found that NLSy1 galaxies, in general, host low-mass black holes ($\sim 10^6 - 10^8 M_\odot$) accreting close to the Eddington limit (Grupe & Mathur 2004; Xu et al. 2012). About 7% of the NLSy1 galaxy population are found to be radio-loud and many of them exhibit compact core-jet radio morphology, flat/inverted radio spectra, high brightness temperature, and superluminal patterns (Komossa et al. 2006; Doi et al. 2006). These features hint for the presence of closely aligned relativistic jets in them and observations from the *Fermi*-Large Area Telescope (*Fermi*-LAT) provided the confirmation. Therefore, it is of great interest to test their similarities/dissimilarities with the blazar class of AGN, which emits copiously in the γ -ray band. The optical and infrared (IR) flux variations of some of these γ -ray emitting NLSy1 (γ -NLSy1) galaxies are found to be similar to

blazars (Liu et al. 2010; Jiang et al. 2012; Paliya et al. 2013a). Variable optical polarization, similar to that known in several blazars is also observed in some γ -ray emitting NLSy1 galaxies (Itoh et al. 2013, 2014). Blazars are known to show hr-scale γ -ray flux variations (e.g., Foschini et al. 2011) and a similar short timescale γ -ray variability was noticed from a NLSy1 galaxy 1H 0323+342 ($z = 0.063$) during its 2013 September outburst (Paliya et al. 2014). A statistically significant curvature is observed in the γ -ray spectra of few γ -NLSy1 galaxies (Paliya et al. 2015) which indicates their resemblance more with the FSRQ class of blazars. The broadband spectral energy distributions (SEDs) of γ -NLSy1 galaxies exhibit the typical double hump structure (e.g., Abdo et al. 2009; D’Ammando et al. 2012; Paliya et al. 2013b), similar to blazars. Additionally, the requirement of external Compton (EC) mechanism to explain the γ -ray window of the SED provides another supporting evidence of the resemblance of these objects with FSRQs (e.g., Abdo et al. 2009; D’Ammando et al. 2012; Foschini et al. 2012; Paliya et al. 2013b).

SBS 0846+513 (R.A.=08:49:58.0, J2000; Decl.=+51:08:28, J2000; $z = 0.585$) is a NLSy1 galaxy found to be a γ -ray emitter by Foschini (2011). *Fermi*-LAT has observed more than one episodes of γ -ray flaring activity from this object where the isotropic γ -ray luminosity reaches as high as 10^{48} erg s⁻¹ (e.g., D’Ammando et al. 2012). Maune et al. (2014) have reported a high amplitude three-magnitude optical flare in 2013 April, closely associated with a high γ -ray state. They also reported the detection of high optical polarization ($\sim 10\%$) during the same period. The very high brightness temperature ($T_b > 10^{13}$ K; Zhou et al. 2005), large amplitude optical variability, and the detection of superluminal motion (D’Ammando et al. 2012) further

hint for the presence of closely aligned relativistic jet in this source. In this work, using all the publicly available multi-wavelength data taken during the first seven years of *Fermi* operation, we study this source in detail. New observations of its intra-night optical variability (INOV) characteristics are also presented. Considering a leptonic origin of radiation, we present a consistent picture of the physical properties of this source.

The paper is organized as follows. We describe the adopted data reduction procedure in section 2. The obtained results are presented and discussed in section 3 followed by the conclusion in section 4. We use the cosmological parameters $\Omega_m=0.27$ and Hubble constant $H_0 = 71 \text{ km s}^{-1} \text{ Mpc}^{-1}$.

2. MULTI-WAVELENGTH OBSERVATIONS AND DATA REDUCTIONS

2.1. *Fermi*-Large Area Telescope Observations

We analyze LAT observations of SBS 0846+513 covering the first seven years of *Fermi* monitoring, i.e., MJD 54683–57222. We follow the standard data reduction procedure as described in the online documentation¹ and here it is briefly mentioned. We use the latest data set (Pass 8) and, in the energy range of 0.1–300 GeV, events belonging to `evclass 128` and `evtype 3` and lying within 15° source region are considered. Data analysis is performed with the package `ScienceTools v10r0p5` along with the use of instrument response functions `P8R2_SOURCE_V6`. To avoid the contamination from Earth limb γ -rays, the maximum zenith angle is adopted as 90° . The region of interest (ROI) is defined as a circle of 10° radius centered at the γ -ray position of SBS 0846+513, as defined in the third catalog of *Fermi*-LAT detected objects (3FGL; Acero et al. 2015). A maximum likelihood test statistics (TS) = $2\Delta\log(\mathcal{L})$, where \mathcal{L} represents the likelihood function between models with and without a point source at the source position, is derived to determine the significance of the γ -ray signal. All the sources present within ROI and defined in the 3FGL catalog are considered for the spectral analysis with their parameters left free to vary during the fitting. In addition to that, objects lying between 10° to 15° from the source of interest, are also included, however, their parameters are kept fixed to the 3FGL catalog values. Galactic and the isotropic extragalactic background emissions are also properly accounted using the latest background templates (`gll_iem_v06.fit` and `iso_P8R2_SOURCE_V6_v06.txt`, respectively). A binned likelihood analysis is performed over the period of interest and all the sources with $\text{TS} < 25$ are removed. This updated model is then used for further temporal and spectral studies.

All the errors associated with the LAT data analysis are 1σ statistical uncertainties, unless specified. Primarily governed by the uncertainty in the effective area, the systematic uncertainties on the measured fluxes are energy dependent: it amounts to 10% at 30 MeV, decreasing linearly as a function of $\log(E)$ to 3% at 100 MeV, and increases linearly as a function of $\log(E)$ beyond 100 GeV to about 15% at 1 TeV².

2.2. *Swift* Telescope Observations

The *Swift* telescope (Gehrels et al. 2004) has observed SBS 0846+513 for a total of 14 times in the first seven years of *Fermi* mission (covering MJD 54683–57222 or 2008 August

4 to 2015 July 15). The source was observed using all the three instruments on board: the Burst Alert Telescope (BAT; Barthelmy et al. 2005, 15–150 keV), the X-Ray Telescope (XRT; Burrows et al. 2005, 0.3–10 keV), and the Ultraviolet/Optical Telescope (UVOT; Roming et al. 2005, 170–600 nm).

SBS 0846+513 is never detected by BAT, primarily due to poor sensitivity of the instrument for short exposures and also due to the low level of hard X-ray emission from the source. Consequently, it is not included in the 70-month *Swift*-BAT hard X-ray catalog (Baumgartner et al. 2013).

We reduce the XRT data following standard procedures available within the HEASOFT package (6.17) and using the latest CALDB files. In particular, the tool `xrtpipeline(v.0.13.1)` is used to perform standard screening and filtering criteria on the data set. All XRT observations were taken in the most sensitive photon counting mode and we use the standard grade selection of 0–12. The calibrated and cleaned event files are summed to generate energy spectra. The source spectra are extracted from a circular region centered at the source and having a radii of $47''$, whereas, the background events are selected from an annular region centered at the source position and having inner and outer radii as $55''$ and $110''$, respectively. We combined the exposure maps using the tool `XIMAGE` and ancillary response files are created with `xrtmkarf` to account for vignetting and PSF corrections. Due to low photon statistics, to perform spectral analysis, we rebinned the spectra to ensure a minimum of 1 count per bin and use Cash statistics (Cash 1979). An absorbed power law (neutral hydrogen column density $N_{\text{H}} = 2.91 \times 10^{20} \text{ cm}^{-2}$; Kalberla et al. 2005) model is used to perform the fitting within `XSPEC` (Arnaud 1996).

The observations from *Swift*-UVOT are integrated using the task `uvotimsum`. Source counts are extracted from a $5''$ circular region centered at the target and background is extracted from a larger area free from source contamination. The source magnitudes are extracted with the task `uvotsource`. Observed magnitudes are then de-reddened for galactic extinction (Schlafly & Finkbeiner 2011). The conversion from corrected magnitudes to flux units is done using the zero points and conversion factors of Breeveld et al. (2011).

2.3. Optical monitoring Observations

The γ -NLSy1 galaxy SBS 0846+513 was observed on a total of six nights between 2012 November and 2013 March as part of our ongoing campaign on NLSy1 galaxies. Three nights of observations were carried out on the 1.3 m telescope located at Devasthal and operated by Aryabhata Research Institute of Observational Sciences (ARIES), India. Another three nights of monitoring was done using the 2 m Himalayan Chandra Telescope at the Indian Astronomical Observatory, located at Hanle, India. All the observations were taken in the *R* band. We follow the standard procedures in `IRAF`³ to perform pre-processing of the images (e.g., bias subtraction, flat-fielding, and cosmic ray removal). The instrumental magnitudes of the target and comparison stars are derived by aperture photometry, using the `phot` task available within the `APPHOT` package in `IRAF`. Following the procedures out-

¹ <http://fermi.gsfc.nasa.gov/ssc/data/analysis/documentation/>

² http://fermi.gsfc.nasa.gov/ssc/data/analysis/LAT_caveats.html

³ `IRAF` is distributed by the National Optical Astronomy Observatories, which is operated by the Association of Universities for Research in Astronomy, Inc. under co-operative agreement with the National Science Foundation.

lined in [Stalin et al. \(2004\)](#), we derived the optimum aperture radius for photometric analysis. First, we generate star–star differential light curves for a series of aperture radii beginning from the median seeing FWHM of that night. The aperture that corresponds to the minimum scatter for the different pairs of comparison stars is selected as the optimum aperture. The positions and apparent magnitudes of the comparison stars (taken from USNO²) used in the differential photometry, are provided in [Table 1](#). It should be noted that uncertainty in the magnitudes of the comparison stars, taken from this catalog, may be up to ~ 0.25 mag ([Monet et al. 2003](#)).

3. RESULTS AND DISCUSSION

3.1. Average γ -ray spectra

The seven years averaged *Fermi*-LAT data of SBS 0846+513 is fitted with both power law (PL) and log parabola (LP) models and the obtained results are presented in [Table 2](#). As can be seen, the fitting of the PL model indicates a relatively harder γ -ray spectrum of SBS 0846+513 ($\Gamma_{0.1-300 \text{ GeV}} = 2.23 \pm 0.03$) compared to other γ -NLSy1 galaxies ([Paliya et al. 2015](#)). The ~ 7 years average γ -ray flux is $(3.79 \pm 0.16) \times 10^{-8} \text{ ph cm}^{-2} \text{ s}^{-1}$ and this corresponds to an isotropic γ -ray luminosity (L_γ) of $\sim 4 \times 10^{46} \text{ erg s}^{-1}$. Such a high L_γ is typically observed from FSRQs (e.g., [Ackermann et al. 2015](#)). The associated significance of detection is $\sim 50\sigma$ (TS ≈ 2635). Moreover, fitting of the LP model hints for the presence of curvature in the γ -ray spectrum ($\beta = 0.11 \pm 0.02$, TS ≈ 2650). In general, powerful FSRQs exhibit a curved γ -ray spectrum (e.g., [Acero et al. 2015](#)) and this indicates the similarity of SBS 0846+513 with FSRQs.

3.2. Multi-wavelength temporal properties

The long term multi-wavelength temporal behavior of SBS 0846+513 is presented in [Figure 1](#). In this plot, the *Fermi*-LAT data points are weekly binned and *Swift* observations are shown as one point per observation Id. Multiple episodes of γ -ray flares are visible and it appears from the available observations that the object brightened at other frequencies also during the period of high γ -ray activity, though it could not be statistically established due to sparseness of the data. The details of these γ -ray flaring behaviors are already described in [Paliya et al. \(2015\)](#) and here we concentrate more on the multi-frequency properties of SBS 0846+513. From the multi-wavelength light curves, we select two high activity periods (F1 and F2) and a quiescent period (Q) for further analysis and SED modeling. The choice of selecting the periods is driven by the availability of multi-frequency data. As can be seen in [Figure 1](#), observations at lower frequencies are not available during the first flare of SBS 0846+513 (before MJD 55800), and thus, this flaring period is not considered for SED analysis. On the other hand, flares during the periods F1 and F2 are simultaneously observed by *Swift*, thus providing an unique opportunity to study them in detail. Interestingly, visual inspection of [Figure 1](#) suggests that the amplitude of γ -ray variability during the periods F1 and F2 seems similar, however, the source appeared brighter during the later period in low frequency *Swift* observations.

3.3. Spectral energy distribution

We generate SEDs for all three periods under consideration ([Figure 1](#)) by averaging the fluxes over each time intervals. In [Table 3](#), we present the associated flux values obtained from this analysis. We model the SEDs by adopting an one zone leptonic emission model described in [Ghisellini & Tavecchio \(2009\)](#) and [Dermer et al. \(2009\)](#) and here we describe it in brief. The emission region is assumed to be spherical, moving relativistically with bulk Lorentz factor Γ at a distance R_{diss} from the central black hole of mass M_{BH} . The semi opening angle of the conical jet is considered as 0.1 rad and the size of the emission region is constrained by assuming it to cover the entire cross-section of the jet. The emission region is filled with the electrons following a smoothly joining broken power law of the form

$$N'(\gamma') = N'_0 \frac{(\gamma'_{\text{brk}})^{-p}}{(\gamma'/\gamma'_{\text{brk}})^p + (\gamma'/\gamma'_{\text{brk}})^q} \quad (1)$$

where p and q are the energy indices before and after the break energy (γ'_{brk}) respectively (primed quantities are measured in the comoving frame). The accretion disk radiation is modeled by assuming a standard optically thick, geometrically thin [Shakura & Sunyaev \(1973\)](#) disk. Locally, its spectrum is assumed as that emitted by a multi-temperature annular blackbody. The broad line region (BLR) is considered as a spherical shell reprocessing 10% of the disk luminosity and emits like a blackbody peaking at the rest-frame Lyman- α frequency ([Tavecchio & Ghisellini 2008](#)). The size of the BLR is assumed to follow the relation $R_{\text{BLR}} = 10^{17} L_{\text{disk},45}^{1/2}$ cm, where $L_{\text{disk},45}$ is the accretion disk luminosity in units of $10^{45} \text{ erg s}^{-1}$ ([Ghisellini & Tavecchio 2009](#)). In our model, the presence of the dusty torus is also considered which reprocesses 50% of the accretion disk emission at IR frequencies. For simplicity, it is assumed to be a thin spherical shell and its emission is considered as a simple blackbody peaking at the temperature T_{IR} . The size of the torus, similar to BLR, scales with the square root of the disk luminosity and assumed to follow the relation $R_{\text{IR}} = 10^{18} L_{\text{d},45}^{1/2}$ cm. In the comoving frame, the radiation energy densities of all the components are computed at the distance R_{diss} from the central black hole following [Ghisellini & Tavecchio \(2009\)](#). The electrons radiate via synchrotron and inverse Compton scattering processes in the presence of a tangled but uniform magnetic field. The synchrotron and synchrotron self Compton (SSC) radiations are derived in the observer's frame, using the prescriptions of [Finke et al. \(2008\)](#). Along with SSC, photons from external components such as the accretion disk, the BLR, and the torus also participate in the IC scattering (e.g., [Dermer et al. 2009](#); [Ghisellini & Tavecchio 2009](#)). The jet powers are calculated following [Celotti & Ghisellini \(2008\)](#). Protons are assumed to carry only the inertia of the jet and do not contribute to the observed radiation. Furthermore, it should be noted that based on H_β line parameters, [Shen et al. \(2011\)](#) estimated the black hole mass of SBS 0846+513 as $\sim 9.77 \times 10^7 M_\odot$. The broadband SED of this object does not show any evidence for the presence of the big blue bump (a characteristic signature of the accretion disk emission), so the observed optical spectrum probably has significant contamination from jet emission not taken into account in [Shen et al. \(2011\)](#), and therefore these estimates should be taken with caution. Recently [Foschini et al. \(2015\)](#) have performed a detailed optical spectroscopic analysis of a sample of NLSy1 galaxies, including SBS 0846+513. They used the H_β line luminosity, instead of

² <http://www.nofs.navy.mil/data/fchpix/>

continuum at 5100 Å, to derive M_{BH} and thus were able to avoid the flux contamination from the host galaxy and the jet. They found M_{BH} of SBS 0846+513 as $3.2 \times 10^7 M_{\odot}$. We reproduce the observed optical-UV part of the SED with a combination of the accretion disk model and synchrotron emission in such a manner so as not to overproduce the observations. With this, we derive a black hole mass as $M_{\text{BH}} = 5.5 \times 10^7 M_{\odot}$ and the disk luminosity as $L_{\text{disk}} = 1 \times 10^{44} \text{ erg s}^{-1}$. Our M_{BH} estimation, via SED modeling, agrees within a factor of two to that derived by Foschini et al. (2015) and therefore, is reliable.

The modeled SEDs are shown in Figure 2 and the associated modeling parameters are given in Table 4. In Figure 2, the red squares represent the simultaneous observations from *Swift* and *Fermi*-LAT and grey circles correspond to archival data⁴.

As can be seen in Figure 2, the SED of SBS 0846+513 has a typical double hump structure, similar to blazars. The synchrotron radiation dominates the observed optical-UV spectra in all the activity states and the contribution from the accretion disk is negligible. This is supported by the detection of a high optical polarization (>10%) during the 2013 April flare (associated here with F2 state) of SBS 0846+513 (Maune et al. 2014). Also, the observed optical-UV spectrum is extremely steep which is difficult to explain by accretion disk model. A high synchrotron emission indicates a high level of SSC emission which is evident in Figure 2. A flat X-ray spectrum is observed which is successfully explained by SSC mechanism. We observed a relatively hard γ -ray spectrum in both the flaring states (see Table 3) which, according to our model, is reproduced by the EC-BLR process. Visual inspection suggests for the possible existence of a break in the γ -ray spectrum which we interpret as a consequence of EC-BLR peak to lie within the LAT energy range. From SED modeling of both the flaring periods, we constrain the location of the emission region to be at the outer edge of the BLR where a major contribution of the seed photons for IC scattering is provided by BLR clouds. These results are different from that obtained by D'Ammando et al. (2012, 2013) where the γ -ray emission is explained on the basis of EC-torus mechanism and the location of the emission region was constrained to be far out from the BLR. Since the emission region is located relatively closer in our case, the derived magnetic fields are higher and the size of the emission regions are smaller compared to them. On the other hand, during the low activity state we found the emission region to be located within the BLR.

3.4. Intra-night optical variability

We observed SBS 0846+513 on a total of six nights between 2012 November to 2013 March, using the 2m Himalayan Chandra Telescope and the 1.3 m telescope at Devasthal. The differential light curves of the NLSy1 galaxy relative to each of the two comparison stars and the comparison stars themselves are shown in Figure 3. The source is considered as variable only when it shows correlated variations both in time and amplitude relative to the selected pair of comparison stars. To quantify INOV, we use two statistical tests, *C*-statistics and *F*-statistics. The *C* parameter is defined as follows

$$C = \frac{\sigma_{\text{T}}}{\sigma_{\text{CS}}} \quad (2)$$

where σ_{T} and σ_{CS} are the standard deviations of the source and the comparison star differential light curves, respectively. The source is considered to have shown INOV if $C \geq 2.576$, which corresponds to 99% confidence level (Jang & Miller 1997). On the other hand, the method of *F*-statistics takes into account the ratio of two variances given as

$$F = \frac{\sigma_{\text{T}}^2}{\sigma_{\text{CS}}^2} \quad (3)$$

where σ_{T}^2 is the variance of source-comparison star differential light curves and σ_{CS}^2 is the variance of the comparison star-star differential light curves. We then compare the derived *F* values with critical *F* value, F_{ν}^{α} , where α is the significance level⁵ and $\nu (= N_p - 1)$ is the degree of freedom from the light curve. We assume the source to be variable only if both the computed *F* values, with respect to the differential light curves of the source to each of the two comparison stars, are greater than the critical *F* value. The results of *F* and *C* statistics are given in Table 5. It should be noted that *C*-statistics might be a more appropriate quantity to check for the presence of variability, especially when the comparison star light curves are not steady. Further, we have not found any correlation between the variability pattern of full width at half maximum (FWHM) of the point source with that observed in the source light curves. Therefore we conclude that the observed INOV are true flux variations of SBS 0846+513. As can be seen in Figure 3 and also in Table 5, the source has shown significant flux variations on all the nights. This suggests a duty cycle of 100%, using both *C* and *F* statistics. The duty cycle is defined as the ratio of the time over which the object shows flux variations to the total observing time. It is calculated as follows

$$DC = 100 \frac{\sum_{i=1}^n N_i (1/\Delta t_i)}{\sum_{i=1}^n (1/\Delta t_i)} \%, \quad (4)$$

where $\Delta t_i = \Delta t_{i,\text{obs}}(1+z)^{-1}$ is the duration of the monitoring session of a source on the *i*th night, corrected for the redshift *z*. N_i is equal to 1 if INOV is detected and otherwise 0. Considering the INOV patterns exhibited by other γ -NLSy1 galaxies, studied in our earlier work (Paliya et al. 2013a, 2014), the overall duty cycle for γ -NLSy1 galaxies is found to be 55% and 81%, according to *C* and *F* statistics, respectively. Such high amplitude ($\psi > 3\%$), high duty cycle ($\sim 70\%$) INOV are generally seen in the BL Lac objects (e.g., Stalin et al. 2004). This supports the idea that the INOV characteristics of γ -NLSy1 galaxies are similar to blazars.

An interesting phenomenon is the observation of INOV behavior of a source during the γ -ray flaring period. It has been shown by Paliya et al. (2014), based on the results of another γ -NLSy1 galaxy 1H 0323+342, that the chances of detecting large amplitude INOV are higher during the γ -ray flaring period. Coincidentally, one of the INOV observations reported here (2013 March 11) was taken during one of the γ -ray flares of SBS 0846+513 (period F2). During this night, the brightness of the source first decreased by ~ 0.3 magnitude and then increased by a similar amount within ~ 7 hrs. (see Figure 3). As can be seen in this plot, on top of the large flare, many small amplitude but fast variations are also visible. Such fast INOV features are also seen in the γ -NLSy1 galaxies 1H 0323+342 and PMN J0948+0022 (Paliya et al. 2013a,

⁴ <http://tools.asdc.asi.it/SED/>

⁵ A significance level of $\alpha = 0.01$ corresponds to a confidence level > 99%.

2014). This hints for the existence of high incidence of INOV during γ -ray flaring activity, and consequently argue for a jet based origin for the observed INOV.

4. CONCLUSIONS

In this work, we present a multi-wavelength study of the γ -ray emitting NLSy1 galaxy SBS 0846+513. The INOV observations reported here are new and the observation on any particular night span more than five hours. We summarize our findings below.

1. The multi-wavelength light curves of the source show multiple episodes of γ -ray flaring activities which are also reflected in lower frequency observations. However, the existence of close correlation between γ -ray and X-ray wavelengths could not be statistically confirmed due to the sparseness of the data.
2. A statistically significant curvature is noticed in the seven years averaged LAT spectrum of SBS 0846+513, a feature generally seen in the γ -ray spectra of powerful FSRQs.
3. The broadband SEDs of SBS 0846+513 show the typical double hump structure, similar to blazars, with a steep optical and a relatively hard γ -ray spectrum.
4. The modeling of the SEDs with a one zone leptonic emission model indicates the optical-UV spectrum to be dominated by synchrotron emission, whereas, the X-ray spectra are well explained by SSC process. The γ -ray regions of the SEDs are explained by IC scattering of BLR photons. It is found that during both the flaring activity states, the emission region was located at the outer edge of the BLR, while during the low activity state it was well within the BLR.
5. Significant INOV is noticed on all the six nights of ground based optical observations. Interestingly, a large amplitude INOV is seen during the γ -ray flaring period F2.

We thank the referee for constructive comments that helped in improving the manuscript. This research has made use of the data obtained from HEASARC provided by the NASA's Goddard Space Flight Center. Part of this work is based on archival data, software or on-line services provided by the ASI Science Data Center (ASDC). This research has made use of the XRT Data Analysis Software (XRTDAS) developed under the responsibility of the ASDC, Italy. Use of *Hydra* cluster at Indian Institute of Astrophysics is acknowledged.

REFERENCES

- Abdo, A. A., Ackermann, M., Ajello, M., et al. 2009, *ApJ*, 707, L142
 Acero, F., Ackermann, M., Ajello, M., et al. 2015, *ApJS*, 218, 23
 Ackermann, M., Ajello, M., Atwood, W. B., et al. 2015, *ApJ*, 810, 14
 Arnaud, K. A. 1996, in *Astronomical Society of the Pacific Conference Series*, Vol. 101, *Astronomical Data Analysis Software and Systems V*, ed. G. H. Jacoby & J. Barnes, 17
 Barthelmy, S. D., Barbier, L. M., Cummings, J. R., et al. 2005, *Space Sci. Rev.*, 120, 143
 Baumgartner, W. H., Tueller, J., Markwardt, C. B., et al. 2013, *ApJS*, 207, 19
 Boller, T., Brandt, W. N., & Fink, H. 1996, *A&A*, 305, 53
 Breeveld, A. A., Landsman, W., Holland, S. T., et al. 2011, in *American Institute of Physics Conference Series*, Vol. 1358, *American Institute of Physics Conference Series*, ed. J. E. McEnery, J. L. Racusin, & N. Gehrels, 373–376
 Burrows, D. N., Hill, J. E., Nousek, J. A., et al. 2005, *Space Sci. Rev.*, 120, 165
 Cash, W. 1979, *ApJ*, 228, 939
 Celotti, A., & Ghisellini, G. 2008, *MNRAS*, 385, 283
 D'Ammando, F., Orienti, M., Finke, J., et al. 2012, *MNRAS*, 426, 317
 —. 2013, *MNRAS*, 436, 191
 Dermer, C. D., Finke, J. D., Krug, H., & Böttcher, M. 2009, *ApJ*, 692, 32
 Doi, A., Nagai, H., Asada, K., et al. 2006, *PASJ*, 58, 829
 Finke, J. D., Dermer, C. D., & Böttcher, M. 2008, *ApJ*, 686, 181
 Foschini, L. 2011, in *Foschini, L. 2011, in Proceedings of Science*, vol. 126, *Narrow-Line Seyfert 1 Galaxies and their Place in the Universe*, ed. L. Foschini, M. Colpi, L. Gallo et al.
 Foschini, L., Ghisellini, G., Tavecchio, F., Bonnoli, G., & Stammera, A. 2011, *A&A*, 530, A77
 Foschini, L., Angelakis, E., Fuhrmann, L., et al. 2012, *A&A*, 548, A106
 Foschini, L., Berton, M., Caccianiga, A., et al. 2015, *A&A*, 575, A13
 Gehrels, N., Chincarini, G., Giommi, P., et al. 2004, *ApJ*, 611, 1005
 Ghisellini, G., & Tavecchio, F. 2009, *MNRAS*, 397, 985
 Goodrich, R. W. 1989, *ApJ*, 342, 224
 Grupe, D., & Mathur, S. 2004, *ApJ*, 606, L41
 Itoh, R., Tanaka, Y. T., Fukazawa, Y., et al. 2013, *ApJ*, 775, L26
 Itoh, R., Tanaka, Y. T., Akitaya, H., et al. 2014, *PASJ*, 66, 108
 Jang, M., & Miller, H. R. 1997, *AJ*, 114, 565
 Jiang, N., Zhou, H.-Y., Ho, L. C., et al. 2012, *ApJ*, 759, L31
 Kalberla, P. M. W., Burton, W. B., Hartmann, D., et al. 2005, *A&A*, 440, 775
 Komossa, S., Voges, W., Xu, D., et al. 2006, *AJ*, 132, 531
 Liu, H., Wang, J., Mao, Y., & Wei, J. 2010, *ApJ*, 715, L113
 Maune, J. D., Eggen, J. R., Miller, H. R., et al. 2014, *ApJ*, 794, 93
 Monet, D. G., Levine, S. E., Canzian, B., et al. 2003, *AJ*, 125, 984
 Osterbrock, D. E., & Pogge, R. W. 1985, *ApJ*, 297, 166
 Paliya, V. S., Sahayanathan, S., Parker, M. L., et al. 2014, *ApJ*, 789, 143
 Paliya, V. S., Stalin, C. S., Kumar, B., et al. 2013a, *MNRAS*, 428, 2450
 Paliya, V. S., Stalin, C. S., & Ravikummar, C. D. 2015, *AJ*, 149, 41
 Paliya, V. S., Stalin, C. S., Shukla, A., & Sahayanathan, S. 2013b, *ApJ*, 768, 52
 Pounds, K. A., Done, C., & Osborne, J. P. 1995, *MNRAS*, 277, L5
 Roming, P. W. A., Kennedy, T. E., Mason, K. O., et al. 2005, *Space Sci. Rev.*, 120, 95
 Schlafly, E. F., & Finkbeiner, D. P. 2011, *ApJ*, 737, 103
 Shakura, N. I., & Sunyaev, R. A. 1973, *A&A*, 24, 337
 Shen, Y., Richards, G. T., Strauss, M. A., et al. 2011, *ApJS*, 194, 45
 Stalin, C. S., Gopal Krishna, Sagar, R., & Wiita, P. J. 2004, *Journal of Astrophysics and Astronomy*, 25, 1
 Tavecchio, F., & Ghisellini, G. 2008, *MNRAS*, 386, 945
 Xu, D., Komossa, S., Zhou, H., et al. 2012, *AJ*, 143, 83
 Yao, S., Yuan, W., Zhou, H., et al. 2015, *MNRAS*, 454, L16
 Zhou, H.-Y., Wang, T.-G., Dong, X.-B., Li, C., & Zhang, X.-G. 2005, *Chinese J. Astron. Astrophys.*, , 5, 41

Table 1
Positions and apparent magnitudes of the comparison stars from the USNO catalog

Star	RA (J2000) (h m s)	Dec. (J2000) (d m s)	R (mag)
S1	08:49:38.49	+51:07:55.52	16.90
S2	08:49:41.34	+51:10:57.97	16.90
S3	08:50:16.73	+51:09:23.36	17.40

Table 2

Seven years averaged LAT data analysis of γ -NLSy1 galaxy SBS 0846+513. Column information are as follows: (1) model used for fitting (PL: power law, LP: log parabola); (2) 0.1–300 GeV flux in units of 10^{-8} ph cm $^{-2}$ s $^{-1}$; (3) power law photon index or log parabolic photon index at pivot energy obtained from fitting the log parabola model; (4) curvature index; (5) TS; and (6) γ -ray luminosity in units of 10^{46} erg s $^{-1}$.

Model	F $_{0.1-300}$ GeV	$\Gamma_{0.1-300/\alpha}$	β	TS	L $_{\gamma}$
(1)	(2)	(3)	(4)	(5)	(6)
PL	3.79 ± 0.16	2.23 ± 0.03	—	2634.82	4.25
LP	3.18 ± 0.19	1.96 ± 0.06	0.11 ± 0.02	2648.15	4.30

Table 3
Summary of SED generation analysis.

		<i>Fermi</i> -LAT				
Activity state	Period ¹	Flux ²	Photon Index ³	Test Statistic ⁴	N $^5_{\text{pred}}$	
F1	56000–56200	9.04 ± 0.61	2.11 ± 0.04	1085.60	1056.01	
Q	56200–56380	1.53 ± 0.56	2.56 ± 0.26	17.32	150.97	
F2	56380–56500	9.92 ± 0.84	2.10 ± 0.05	732.15	658.01	
		<i>Swift</i> -XRT				
Activity state	Exp. ⁶	Photon index ⁷	Flux ⁸	Normalization ⁹	Stat. ¹⁰	
F1	4.75	1.45 ± 0.28	$1.02^{+0.32}_{-0.21}$	1.15 ± 0.26	81.42/77	
Q	19.14	1.61 ± 0.23	$0.39^{+0.10}_{-0.07}$	0.52 ± 0.01	105.14/131	
F2	7.63	1.34 ± 0.16	$1.68^{+0.31}_{-0.25}$	1.69 ± 0.23	142.28/177	
		<i>Swift</i> -UVOT				
Activity state	V ¹¹	B ¹¹	U ¹¹	W1 ¹¹	M2 ¹¹	W2 ¹¹
F1	3.67 ± 0.20	2.71 ± 0.13	1.82 ± 0.09	0.95 ± 0.06	1.02 ± 0.06	0.79 ± 0.04
Q	0.62 ± 0.10	0.39 ± 0.06	0.18 ± 0.06	0.16 ± 0.02	0.16 ± 0.02	0.14 ± 0.01
F2	7.57 ± 0.26	5.81 ± 0.23	3.82 ± 0.18	2.35 ± 0.15	2.80 ± 0.17	1.86 ± 0.10

¹Time interval considered for SED modeling, in MJD.

²Integrated γ -ray flux in 0.1–300 GeV energy range in units of 10^{-8} ph cm $^{-2}$ s $^{-1}$.

³Photon index calculated from γ -ray analysis.

⁴Significance of detection using likelihood analysis.

⁵Number of predicted photons during the time period under consideration.

⁶Net exposure in kiloseconds.

⁷Photon index derived from X-ray analysis.

⁸Observed flux in units of 10^{-12} erg cm $^{-2}$ s $^{-1}$, in 0.3–10 keV energy band.

⁹Normalization at 1 keV in 10^{-4} ph cm $^{-2}$ s $^{-1}$ keV $^{-1}$.

¹⁰Statistical parameters: C-stat./dof.

¹¹Average flux in *Swift* UVOT bands in units of 10^{-12} erg cm $^{-2}$ s $^{-1}$.

Table 4

Summary of the parameters used/derived from the SED modeling. Viewing angle is assumed as 3° and the characteristic temperature of the dusty torus as 900 K. For a disk luminosity of 1×10^{44} erg s $^{-1}$ and black hole mass of $5.5 \times 10^7 M_\odot$, the size of the BLR is 0.01 parsec ($1947 R_{\text{Sch}}$).

Parameter	Symbol	F1	Q	F2
Particle spectral index before break energy	p	1.8	1.9	1.8
Particle spectral index after break energy	q	7.0	7.2	7.0
Magnetic field in Gauss	B	3.5	4.2	3.9
Particle energy density in erg cm $^{-3}$	U'_e	0.40	0.70	0.42
Bulk Lorentz factor	Γ	13	7	13
Break Lorentz factor of electrons	γ'_{brk}	1088	1047	1278
Maximum Lorentz factor of electrons	γ'_{max}	3e4	3e4	3e4
Distance of the emission region in parsec (R_{Sch})	R_{diss}	0.011 (2100)	0.009 (1700)	0.011 (2100)
Jet power in electrons in log scale	P_e	43.87	43.39	43.89
Magnetic jet power in log scale	P_B	43.95	43.38	44.05
Radiative jet power in log scale	P_r	44.50	43.81	44.66
Jet power in protons in log scale	P_p	46.04	45.69	46.05

Table 5

Log of INOV observations of SBS 0846+513. Column information are as follows: [1] observation date; [2] INOV amplitude in percent; [3] and [4] C -values computed for differential light curves relative to the steadiest pair of comparison stars; [5] variability status according to C -statistics, V: variable, NV: non-variable; [6] and [7] Values of F parameter for the differential light curves relative to the two comparison stars; and [8] variability status as per F -statistics.

Date	ψ	CI	$C2$	Status	$F1$	$F2$	Status
yyyy mmm dd	(percent)	[3]	[4]	[5]	[6]	[7]	[8]
2012 Nov 20	11.99	2.62	2.93	V	6.85	8.60	V
2012 Dec 9	24.37	6.98	6.88	V	48.78	47.33	V
2012 Dec 10	22.15	3.32	2.92	V	11.00	8.53	V
2012 Dec 25	41.30	4.55	4.51	V	20.67	20.32	V
2013 Feb 12	36.76	7.56	7.91	V	57.15	62.50	V
2013 Mar 11	33.27	7.91	7.64	V	62.53	58.38	V

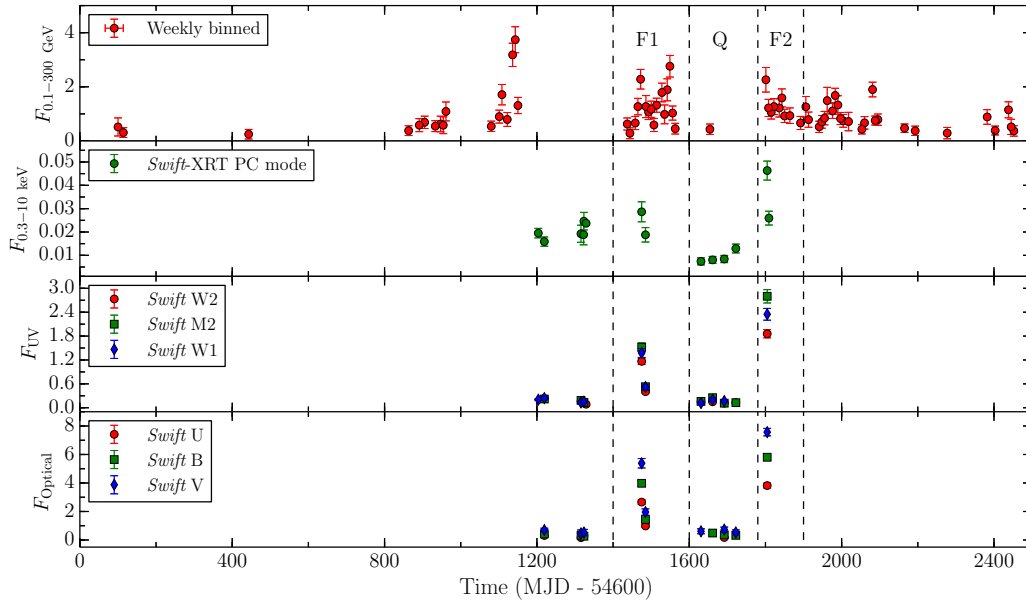


Figure 1. Multi-wavelength light curves of SBS 0846+513 covering the period 2008 August to 2015 July. Top panel represents the weekly binned γ -ray light curve with flux units of 10^{-7} ph cm $^{-2}$ s $^{-1}$. Remaining three panels correspond to *Swift* observations binned as one point per observation Id. *Swift*-XRT data points are in units of counts s $^{-1}$ and *Swift*-UVOT observations are in units of 10^{-12} erg cm $^{-2}$ s $^{-1}$. F1 and F2 are two high activity periods and Q represents a low activity state, selected for SED modeling. See the text for details.

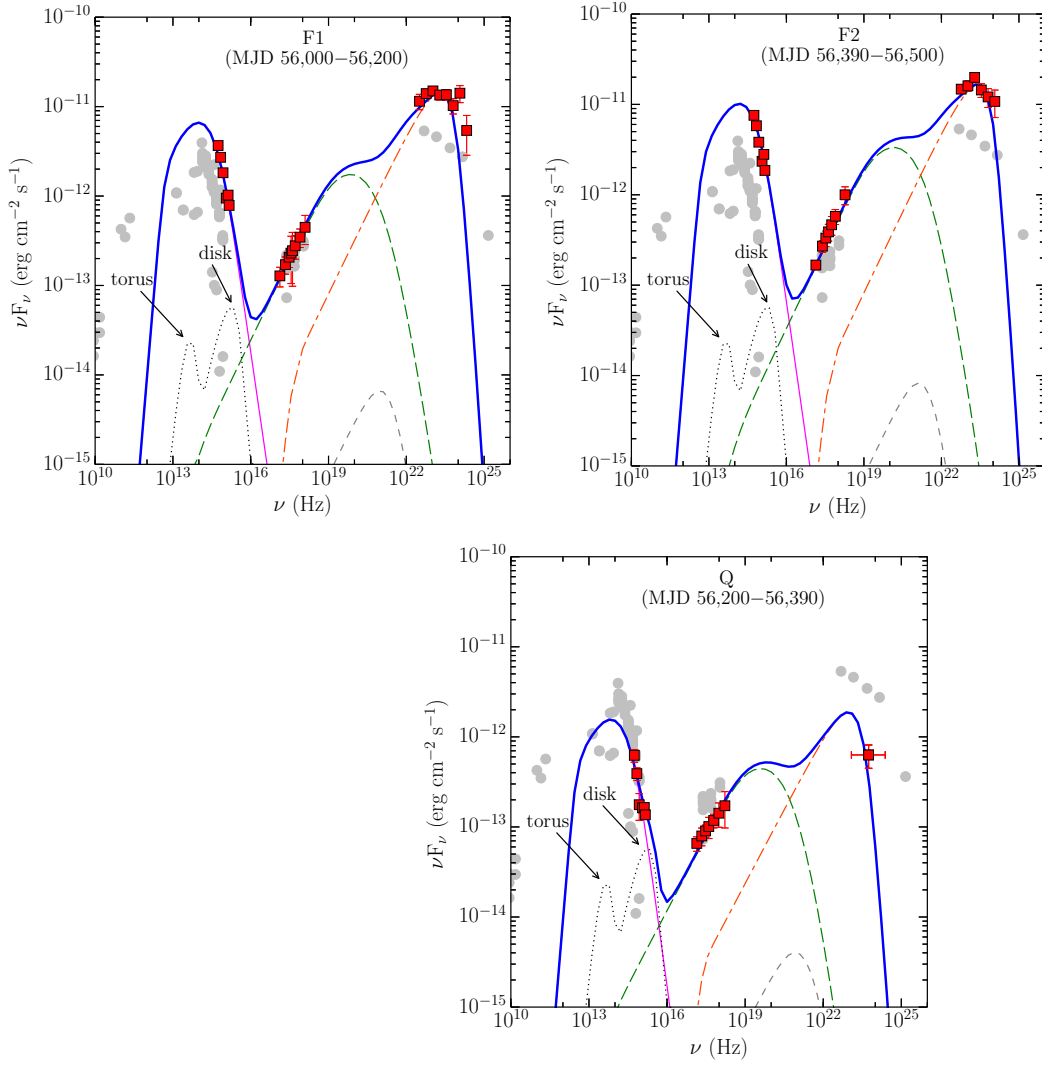


Figure 2. SEDs of SBS 0846+513 during various activity states. Red squares are the simultaneous observations from *Swift* and *Fermi*-LAT, whereas, grey circles represent the archival observations. Thermal radiations from the accretion disk and the torus are shown by dotted black line. Pink thin solid, green long dashed, orange dash-dash-dot, and grey dashed lines correspond to synchrotron, SSC, EC-BLR, and EC-torus emissions, respectively. Blue thick solid line is sum of all the radiative components.

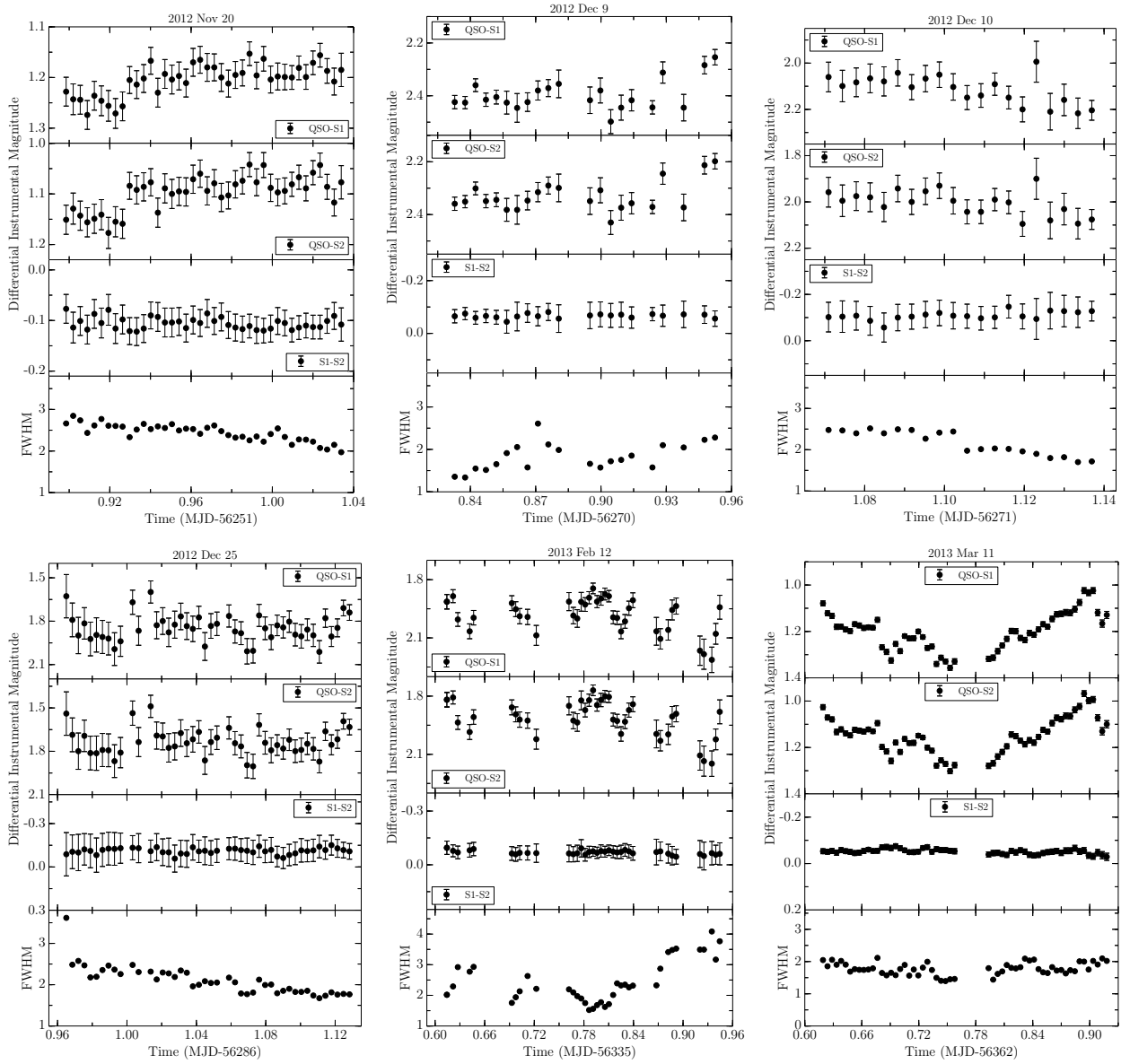


Figure 3. Intra-night differential light curves of SBS 0846+513. On the bottom panel of each plot is given the variations of the FWHM of the stellar images during the night. QSO refers to the source SBS 0846+513, while S1 and S2 denote the two comparison stars selected to generate the differential light curves.